Polarization sensitive coherent anti-Stokes Raman scattering spectroscopy of the amide I band of proteins in solutions

Andrey Yu. Chikishev,* Gerald W. Lucassen,‡ Nikolai I. Koroteev,* Cees Otto,‡ and Jan Greve‡

*International Laser Center, Moscow State University, Lenin Hills, 119899 Moscow, Russia; and ‡Biophysical Technology Group, Department of Applied Physics, University of Twente, 7500 AE Enschede, The Netherlands

ABSTRACT   Polarization sensitive coherent anti-Stokes Raman scattering (PCARS) spectroscopy is a fruitful technique to study Raman vibrations of diluted molecules under off-electron resonant conditions. We apply PCARS as a direct spectroscopic method to investigate the broad amide I band of proteins in heavy water. In spontaneous Raman spectroscopy, this band is not well resolved. We fit a number of spectra taken of each protein under different polarization conditions, with a single set of parameters. It then appears that some substructure is observed in the amide I band. From this substructure, we determine the percentage of α-helix, β-sheet, and random coil for the proteins lysozyme, albumin, ribonuclease A, and α-chymotrypsin.

INTRODUCTION

It is well known that spontaneous Raman scattering spectroscopy (SRS) is successfully applied in the study of secondary structure of proteins. The results are usually extracted from an analysis of the amide I band. The amide I is a broad band present in Raman spectra of all proteins and polypeptides at 1,640–1,680 cm^{-1} with a full width at half maximum of ~30–40 cm^{-1}. This band is associated primarily with the stretching vibration of the peptide carbonyl group which is sensitive to the secondary structure of the polypeptide.

In one of the first papers on Raman spectroscopy of polypeptides (1), it was shown that the position of the amide I band is different for the different types of secondary structure. Studying poly-L-lysine, the authors showed that for an α-helical conformation the amide I band lies at 1,645 (aqueous solution) or 1,632 cm^{-1} (solution in heavy water); for β-sheet it is positioned at 1,670 or 1,658 cm^{-1}, respectively; and for random coil it lies at 1,660 cm^{-1} for the solution in heavy water. In normal water the random coil position cannot be assigned because this region is blocked by a broad water contribution.

Position and shape of the amide I band are characteristic for each protein. Many authors analyzed the amide I band of proteins by deconvolving it to obtain information on the contributions of the different secondary structures. One of the first variants of such an analysis was implemented by Lippert et al. (2), who solved a system of linear equations depending on the signal intensities at definite positions in the Raman spectra of several proteins. The intensities of the Raman spectra of poly-L-lysine, in different conformations, were used as reference set. Later, Williams and Dunker (3) suggested another variant of such an analysis which has been improved further in the work of Williams (4). These authors have introduced the application of calculated spectra of basic structures which are used for the deconvolution of the amide I band. A more general approach, the reference intensity profile method, was proposed by Berjot et al. (5). The reference profiles of the secondary

structure elements were calculated with the help of a fit procedure for the amide I band of a large number of proteins with known conformations. Later, these methods were applied for analysis of the secondary structure of specific proteins (6–9). Similar approaches were used in infrared spectroscopy (10, 11).

The Raman spectra of the amide I band presented in the literature cited above display practically no internal structure. Fig. 1 shows a measured spontaneous Raman spectrum of lysozyme in heavy water in the amide I region. Yet it is clear that at least three different conformations, corresponding to α-helix, β-sheet, and random coil, contribute to this band. If different forms of turns are taken into account, then even more separate spectral contributions may be expected. Although the accuracy of the analysis of Raman spectra in the amide I region is high and the results obtained are in reasonable agreement with existing x-ray and circular dichroism (CD) data, it would be preferred if direct spectroscopic information about the internal structure of the amide I band could be obtained.

In the last decade, nonlinear Raman spectroscopy made rapid progress. One of the variants of this spectroscopy, based on four wave mixing, is coherent anti-Stokes Raman scattering (CARS), which has been applied successfully to the investigation of large organic and biomolecules (12–19). Like SRS, CARS gives information on molecular vibrations. Although this method is rather difficult in implementation as compared with SRS, it has several important advantages: high spectral resolution limited only by the line widths of the lasers being used (for dye lasers, typically 0.1–0.5 cm^{-1}), a high collection efficiency because of the coherent (laserlike) signal character, the absence of a luminescent background (registration in the anti-Stokes part of the spectrum), and high intensity of the signal (several orders of magnitude higher than in SRS) (20).

The major shortcoming of CARS is the presence of a strong coherent nonresonant background arising mainly from the solvent molecules. This background is a serious
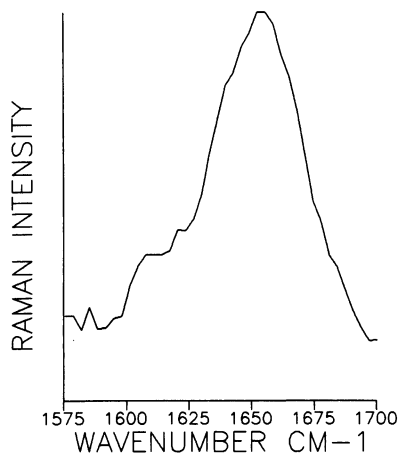
FIGURE 1 Amide I band of 50 mg/ml lysozyme in D_2O measured by spontaneous Raman.

problem for the investigation of proteins in solution. However, there exists methods allowing to suppress the nonresonant background in CARS experiments. One of them is the polarization sensitive variant of CARS (PCARS).

PCARS possesses a number of additional advantages based on the holographic nature of the four wave mixing scheme (21, 22). By using polarizers in the excitation and registration paths of the PCARS signal and variation of their relative orientation ϵ, introduction of an additional spectroscopic coordinate to the ones normally used (intensity and frequency) is obtained. The PCARS spectrum becomes "three dimensional" because of the mixing of nonresonant and resonant scattering signals that express the holographic nature of PCARS (21). By varying the angle ϵ, the experimenter can actively control the relative amplitudes and phases of different contributions to the experimentally observed CARS spectra. This provides the opportunity of "viewing" complex Raman bands from different directions and allows for the determination of relative phases of vibrational and background scattering.

Despite the advantages mentioned above, the PCARS spectroscopy in its off-electron resonant variant has not been applied widely to the investigation of proteins and polypeptides in solution. Some examples of such studies with other molecules of biological importance may be found in references (12, 14, and 18). Therefore, we planned this study as a new direct spectroscopic approach to investigate the secondary structure of proteins.

EXPERIMENTAL

Lysozyme (from egg-white, no. 120007 623-80, crystallized (hydrochloride), human albumin (no. A-8763), and ribonuclease A (from bovine pancreas, no. 34388) were obtained from Sigma Chemical Co., St. Louis, MO. Chymotrypsin was kindly provided by Dr. Yu. I. Khurgin (Institute of Organic Chemistry, Russian Academy of Science) and used without further purification. The proteins were dissolved in heavy

water to obtain concentrations of 25–200 mg/ml. Heavy water instead of normal water was used in our experiments to avoid the overlapping vibrations of normal water and the amide I band of the proteins in the 1,600–1,700 cm^{-1} region. According to Blout et al. (23), 85–90% deuterium exchange with amide protons takes place in 3 h. The PCARS spectra were recorded not earlier than 3 h after sample preparation. During that time, the solutions were kept in a refrigerator under sterile conditions at 4°C.

The CARS spectrometer consists of a Nd:YAG laser (Quanta Ray, DCR-2, 10-Hz repetition rate, 10-ns pulse duration, 300 mJ at 1,064 nm) which pumps a PDL2 dyelaser at the second harmonic at λ = 532 nm. The dyelaser contained rhodamine 610, delivering the Stokes beam at wavelengths 580–640 nm, thus covering the 1,400–1,800 cm^{-1} region of the measurements.

About 10% of the 532-nm beam is used as pump beam in the degenerate CARS scheme. The pump and Stokes beam diameters are compressed by telescopes to 2 mm, and part of the beams is split off and detected by photo diodes for intensity monitoring. The polarizations of the beams were set by high quality Glan-Taylor prisms (extinction ratio 10^{-7} at crossed polarizations). The Stokes beam was directed parallel to the pump beam onto the focusing lens (250 mm) by means of a mirror mounted on a stepper motor-driven translation stage to control the phase-matching angles via the distance of the beams (see Fig. 2). The polarization of the Stokes beam was adjusted almost parallel to this mirror interface to achieve minimum depolarization. The polarization of the pump beam could be adjusted to any desired angle by use of a half wave retardation plate at 532 nm and the Glan-Taylor prism directly thereafter. The CARS signal was analyzed by a Glan-Taylor polarizing prism.

The relative polarizer settings could be acquired with high precision by means of micrometer screws on the polarizer prism rotator holder. The greatest uncertainty with the polarization setting is the absolute angle reading (with large angle settings $\Delta\alpha \simeq 0.5°$, whereas relative angle settings could be done within 0.01°).

The pump and Stokes beams are focused in protein solutions held by two microscope cover glass slides, which were antireflection coated at their air-glass interface to minimize multiple interference effects (24). The signal coming from the cuvet glass layers is negligible compared with that of the sample layer. The sample is positioned on the rotation axis of a signal collection rotator. The CARS signal is reflected back onto this rotation axis at every collection angle position of the collector arm and is mirrored into the entrance slit of the double monochromator (UV-VIS Jobin Yvon 250 mm, holographic gratings). The monochromator output is directed on a photomultipliertube (model 9973B; RCA). The computer and electronics are connected via an IEEE bus interface. The signals are digitized in an 8-channel 12-bit analogue to digital converter (ADC) and stored on floppy disks for analysis. Automatic wavelength selection of the dyelaser and monochromator, matching, and collection at the desired wavenumber shift are achieved by computer control of the stepper motors and predetermined angle files for the solutions.

The energies of the beams were 400 μJ/pulse at the sample. The focal beam diameter at the sample was $\sim$200 μm. The spectra were recorded in two parts: from 1,400 to 1,600 and 1,600 to 1,800 cm^{-1} with 200 points and 30 averages per spectrum point. A scan of 200 points took $\sim$20 min. The spectra shown are smoothed by a five- to seven-points Savitsky-Golay smoothing procedure.

PCARS METHOD

The degenerate (two-color) CARS method uses two laser beams, one with a fixed frequency, ω_p (pump beam), and one with variable frequency, ω_s (Stokes beam). In Fig. 3 the four-photon process is depicted in an energy level diagram. Two pump photons, ω_p, and one Stokes photon, ω_s, generate a CARS signal photon,
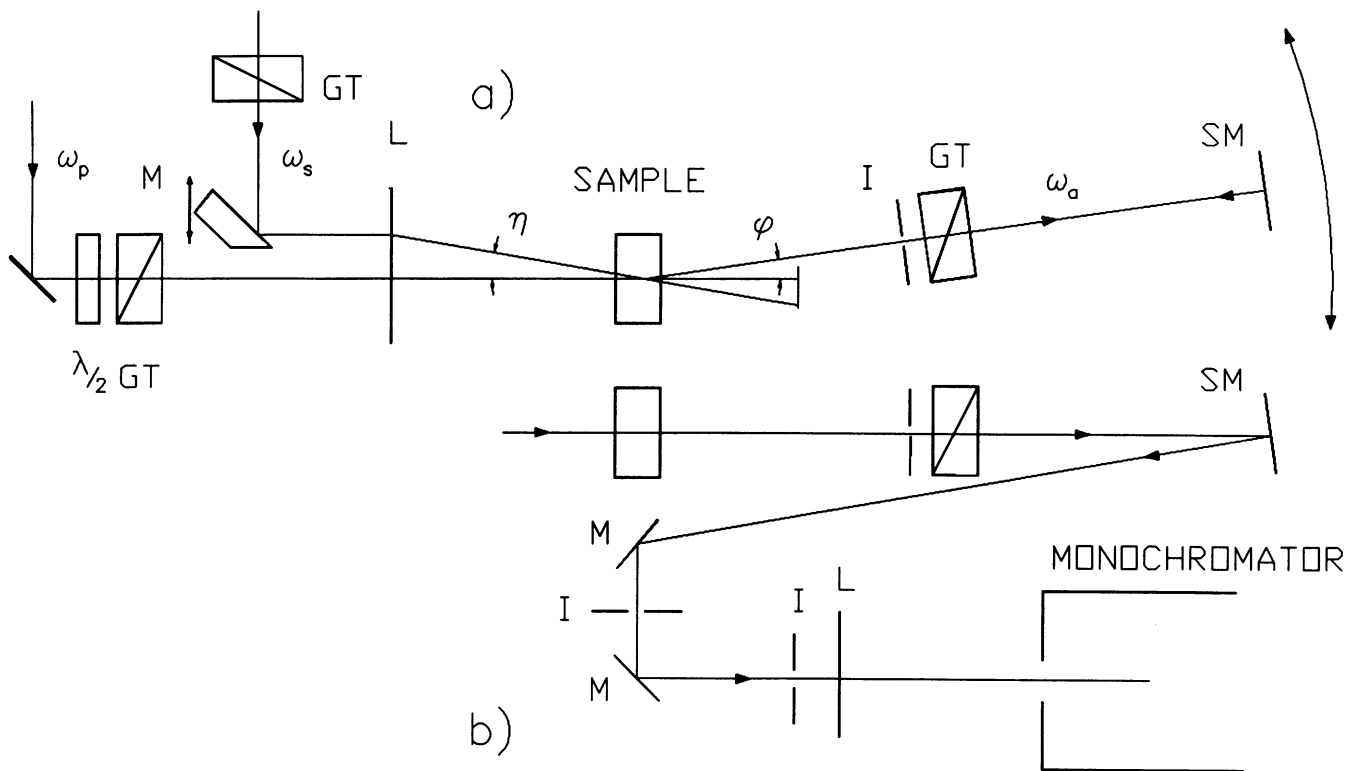
FIGURE 2 Detail of the polarization CARS setup, (*a*) top view and (*b*) side view, of the collection rotator. *GT*, Glan-Taylor prism; *I*, iris diaphragm; *M*, mirror; η, phase-matching angle input beams; *L*, lens; and ϕ, signal collection angle.

ω_a at $\omega_a = 2\omega_p - \omega_s$ (energy conservation). The frequency ω_s is scanned across the vibrations of interest. Different four-photon processes contribute to the total signal. They can be divided (see Fig. 3) in (*a*) vibration resonant contributions, where the difference $\omega_p - \omega_s$ equals a vibrational resonance at ω_r, and (*b*) nonvibration resonant contributions. For both cases (resonant and nonresonant), the signal frequency is $\omega_a = \omega_p + (\omega_p - \omega_s)$. Because of energy and momentum conservation, a maximum signal is obtained at direction $k_a = 2k_p - k_s$. The matching angle η between k_p and k_s and the collection angle ϕ between k_p and k_a are predetermined for different frequencies and stored in angle files to use in the computer program.

The incoming electric fields $\mathbf{E}_{p,s}$ induce a polarization **P** in the sample that acts as a source to generate the signal CARS field $\mathbf{E}_a$. The nonlinear CARS process is generated via

$$\mathbf{P}^{(3)} = \chi^{(3)}\mathbf{E}_p\mathbf{E}_p\mathbf{E}_s^*, \tag{1}$$

with $\mathbf{P}^{(3)}$ the total polarization

$$\mathbf{P}^{(3)} = \mathbf{P}^{(3)N} + \mathbf{P}^{(3)R} \tag{2}$$

arising from the nonresonant and vibration resonant processes.

The spectral information is contained in the third order nonlinear susceptibility

$$\chi^{(3)}(\omega_a) = \chi^{(3)N} + \chi^{(3)R}(\omega_a). \tag{3}$$

The correspondence between spontaneous Raman and CARS is that the Raman intensity is proportional to the imaginary part of $\chi^{(3)}$.

Detecting the CARS polarization signal $\mathbf{P}^{(3)}$ with an analyzer $\mathbf{e}_A$, the PCARS intensity $I_A(\omega_a)$, arising from the sample at matching conditions, can be written as

$$I_A(\omega_a) \sim |(\mathbf{e}_A^* \cdot \chi^{(3)}_{Apps}(\omega_a)\mathbf{e}_p\mathbf{e}_p\mathbf{e}_s^*)|^2 I_p^2 I_s L^2, \tag{4}$$

where $\mathbf{e}_p$, $\mathbf{e}_s$, and $\mathbf{e}_A$ are the pump, Stokes, and analyzer unit polarization vectors, $\chi^{(3)}_{Apps}$ are the $\chi^{(3)}$ components, I_p and I_s are the pump and Stokes beam intensities. L is the overlap length of the pump and Stokes beams in the sample. Generally, the vibration resonant polarization vector and the nonresonant polarization vector have different orientations (see Fig. 4 and Appendix).

In practice, the absolute value of the vibration resonant polarization of a dilute sample under study is often much smaller than the nonresonant polarization $|\mathbf{P}^R| \ll |\mathbf{P}^{NR}|$ under off-electron resonant excitation conditions. This means that suppression of $\mathbf{P}^{NR}$ is necessary to detect the vibrations of the sample. In isotropic solvents, full suppression of the nonresonant polarization is achieved at angle
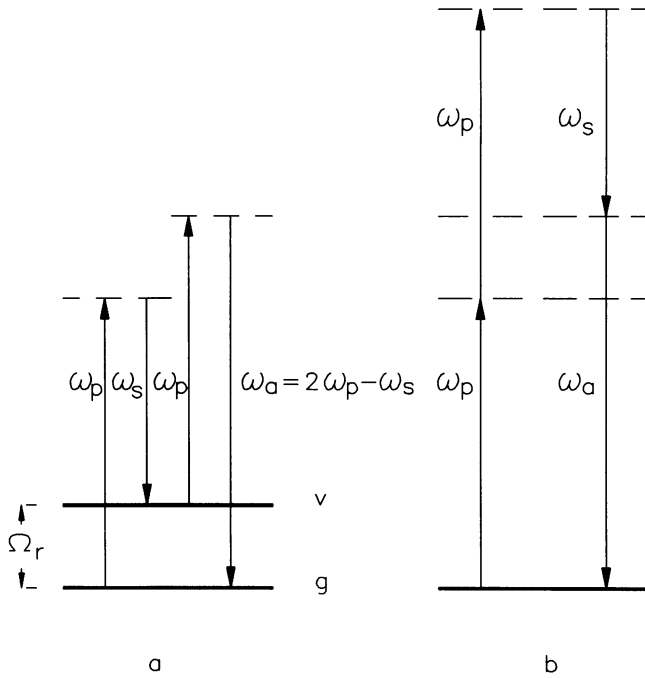
FIGURE 3 Energy level diagram of contributions to the degenerate CARS process: (a) vibration resonant term; (b) example of a nonresonant term. g denotes the electronic groundstate and v the vibrational state.

$$\psi_0 = \arctan\,(3/\tan\,\alpha), \tag{5}$$

where α is the angle between the pump and the Stokes polarization vectors. The projection of the vibration resonant polarization on the analyzer orientation is transmitted as a (background free) signal. By rotation of the analyzer ϵ around the angle ψ_0 of best background suppression, the vibration resonant signal is "heterodyned" with a controlled amount of nonresonant signal.

PCARS FIT PROGRAM

The model used to fit the PCARS spectra in the least-squares procedure is given by

$$F(x) = \chi(x)\chi^*(x), \tag{6}$$

where

$$\chi(x) = \left(f^N \chi^N + \sum_r f^R_r \frac{A_r}{(\Omega_r - x)\gamma_r - i} \right) C \tag{7}$$

with f^N, f^R_r and χ^N defined in Eqs. A9, A10, and A7; A_r, vibration resonant amplitude; Ω_r, vibration resonant frequency; x, a variable representing the frequency shift $\omega_1 - \omega_2$; γ_r, inverse bandwidth $1/\Gamma_r$, and C, scaling parameter.

The fit program enables us to simultaneously fit several spectra measured at different polarization conditions with a single set of parameters to minimize systematic errors. Furthermore, all parameters given in the fit

function Eqs. 6 and 7 can be used as free fit parameters. This enables us to fit different bands with different depolarization ratios and different line shapes. The problem to be solved is to find the minimum of

$$\sum_j \sum_i (I_j(x_i) - F_j(x_i))^2, \tag{8}$$

where $I_j(x_i)$ are measured PCARS intensities at spectrum points x_i at polarization condition j and $F(x)$ defined in Eq. 6.

The total background consists of the non- (electron) resonant susceptibility and the vibration resonant contributions from the solvent (heavy water). At different analyzer settings, ϵ, around the position of best background suppression, it appeared that this background showed dispersive character (a frequency dependent background). The choice for heavy water as a solvent instead of normal water was to avoid a large water vibration resonant signal around $1{,}600$ cm^{-1}; however, the Raman vibrations of heavy water at $1{,}200$, $1{,}500$ (weak), and $2{,}490$ cm^{-1} (strong) cannot be neglected and are included in the fit.

In principle, depolarization ratios can be fitted as well. From the line shape changes in the spectra, it can be deduced (18, 20) whether the bands are polarized ($0 < \rho^R < \rho^{NR} \approx \frac{1}{3}$) or depolarized ($\rho^{NR} < \rho^R < \frac{3}{4}$). However, the large influence of the background in the spectra limits the range of the possible analyzer angle variation (to values $|\epsilon| \leq 1.5°$). Thus, it is difficult to determine depolarization ratios ρ^R accurately. For reasons of simplicity, we limit the iterative process of fitting depolarization ratios to the first step by setting $\rho^R = 0$ for polarized and $\rho^R = 0.75$ for depolarized bands.

RESULTS

PCARS spectra were measured of four proteins in solution at different settings of the analyzer (ϵ). As the PCARS signal intensity is proportional to the protein
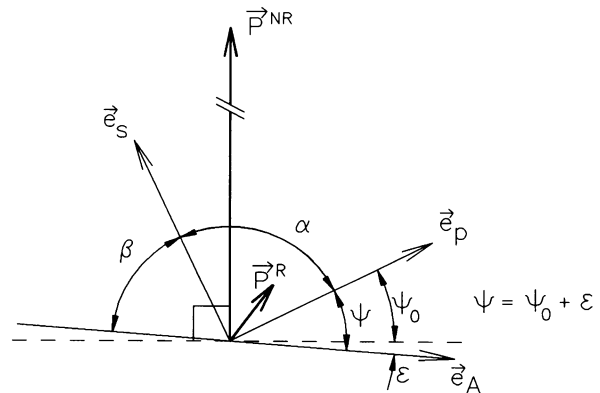

FIGURE 4 Polarization vectors configuration; α angle between pump e_p and Stokes e_s beam polarization, β angle between Stokes beam and analyzer e_A polarization.

concentration, the best signal to noise ratios were obtained for the highest concentration (200 mg/ml). Spectra of reasonable quality could be obtained within the concentration range 25–100 mg/ml.

The most significant feature of the PCARS spectra distinguishing them from the SRS spectra is the dramatic bandshape change observed on changing the polarization conditions. This is illustrated in Fig. 5, where spectra of α-chymotrypsin are presented. It should be emphasized that these spectral recordings differ by only one experimental parameter: the angle ε. Similar spectral series were obtained for all other proteins. It is clearly seen that PCARS allows us either to suppress or to increase the contributions of different vibrational bands to the spectrum.

In Fig. 6, PCARS spectra of albumin, chymotrypsin, and ribonuclease measured in the amide I region are presented, depicting clearly the substructure of the amide I band. The polarization conditions for all spectra presented are similar.

The spectra presented in Fig. 7 are measured at different (as compared with Fig. 6) settings of the analyzer. The obvious shift of the amide I band, indicated by the arrows, as well as the considerable change of the bandshape is due to the interference of nonresonant background and vibrational resonant signal as measured by PCARS. The spectra are therefore strongly dependent on the polarization conditions.

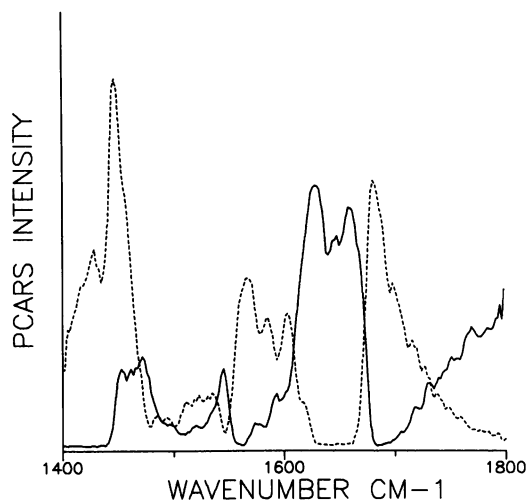One may see from the results presented in Figs. 5–7 that direct extraction of spectral information from the

FIGURE 5   PCARS spectra of 200 mg/ml chymotrypsin in D_2O with $\beta = 60°$, ———, $\alpha = 69.6°$; and - - -, $\alpha = 71.8°$. In this scheme, the angle α between pump beam polarization e_p and the Stokes beam polarization e_s was varied at a constant analyzer polarization orientation e_A. The effect is a rotation of the nonresonant polarization with respect to the analyzer polarization vector, or in other words, variation of the angle ε between the nonresonant polarization and the analyzer polarization.
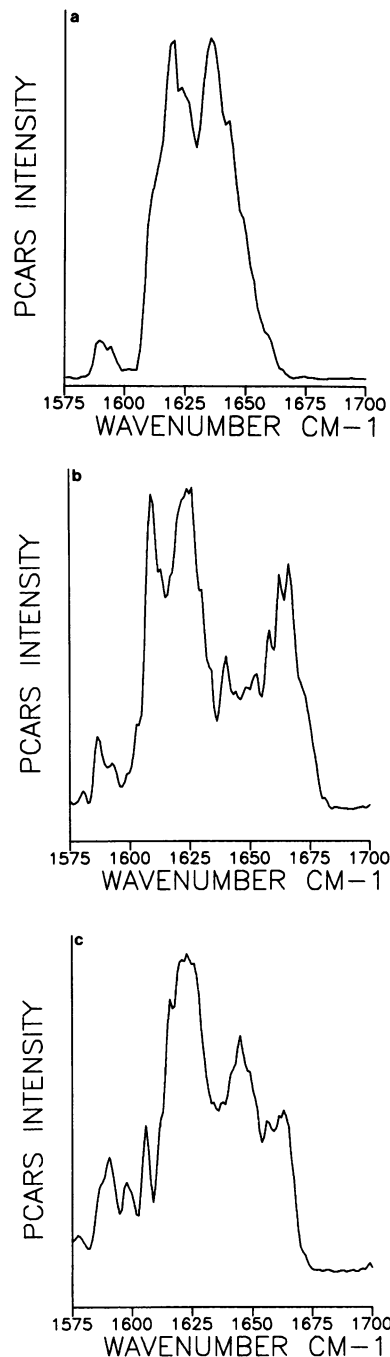

FIGURE 6   PCARS spectra of 200 mg/ml protein in D_2O with $\beta = 60°$, (a) albumin $\alpha = 70.5°$, (b) chymotrypsin $\alpha = 70.4°$, (c) ribonuclease A $\alpha = 70.2°$.

PCARS spectra is rather difficult, especially in the case of overlapping bands. Although the substructure of the amide I band is quite clearly seen at definite polarization conditions, to get quantitative information from the spectra it is necessary to carry out a fit on the spectra with the procedure discussed hereafter. Due to the interference character of the coherent nonlinear signal, it is important to fit not only the bands of interest but also neigh-
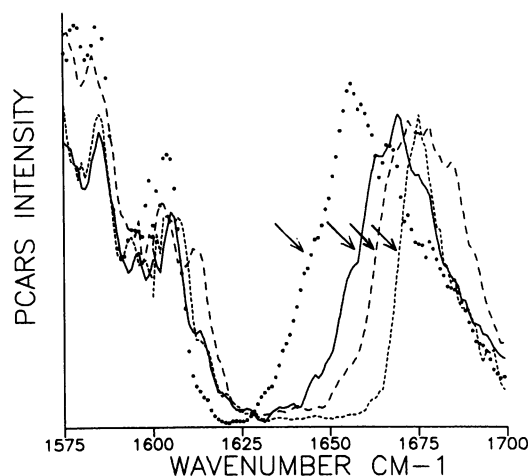
FIGURE 7 PCARS spectra of 100 mg/ml protein in D_2O with $\alpha = 70°$. $\circ\circ\circ$, albumin, $\beta = 59.16°$, 59% (2, 25, 26); ——, lysozyme, $\beta = 59.29°$, 46% (27); ---, ribonuclease A, $\beta = 59.23°$, 22% (27); $\cdots$, chymotrypsin, $\beta = 59.18°$, 10% (27). Note the shifting slope of the bandposition between 1,625 and 1,675 cm^{-1} indicated by arrows for the different proteins. In this scheme, the pump polarization vector e_p and the Stokes polarization vector e_s are fixed (thus a constant angle α between them) and the analyzer polarization e_A (or the angle ϵ) was varied.

boring bands. For this reason we used in our fit a wide spectral range covering not only amide I but several other bands as well.

The results of the PCARS spectral fits for ribonuclease and lysozyme are presented in Fig. 8. The major discrepancies between the experimental and calculated spectra are observed at either low- or high-frequency parts, which is explained by the influence of the solvent vibrations lying outside the measured spectral range.

When starting the fit, we have used existing assignments of Raman bands in spectra of proteins (27, 28) as input for the fit program. To fit the amide I band, we used three bands. This choice was based on the direct spectroscopical information (see Fig. 6). The results of the fit for the four proteins are summarized in Table 1.

The accuracy of the determination of the vibration resonant frequencies and bandwidths is ~ 1 cm^{-1} and is in the order of 30% or less for the amplitudes. This can be deduced from a calculation of a standard least-squares test with variation of the amplitude parameter while keeping the other parameters fixed.

DISCUSSION

The direct spectroscopical data (Figs. 6 and 7) along with the results of the fitting procedure for the PCARS spectra of four proteins clearly indicate that the amide I band consists of at least three bands. The positions of these bands as well as the bandwidths are approximately the same for all proteins, but the relative intensities are

different. In case of albumine, however, the intensity of the third band (highest frequency) is almost negligible (see Table 1), which means that the fit is possible with two bands in the amide I region. These two bands are found at positions corresponding to two of the three bands found in the other proteins.

It remains possible that more than three bands are present in this spectral region because the fit would be even better if additional bands were introduced. In our experiments, we did not see any direct evidence for the presence of these additional bands, however.

It is worthwhile to mention the correlation between the position of the low-frequency slope of the amide I band measured around 1,650 cm^{-1} with the α-helical content in the corresponding protein (see Fig. 7). It is difficult to derive a quantitative correlation between these two values, but this may become possible if additional data are obtained.

The positions of the bands detected in the spectra coincide well with those of the secondary structural elements (α-helix, β-sheet, random coil) presented by different authors (1, 3, 5, 7, 8). The absence (or very small contribution) of a third band in the PCARS spectra of albumine is also in good agreement with the very low content of β-sheet in this protein.

The bands inside the amide I region could only be fitted as polarized (i.e., $0 < \rho^R < \frac{1}{3}$). By choosing definite depolarization ratios ($\rho^R = 0$) for these bands, a possible systematic error may have been introduced. The choice of different depolarization ratios results in different values of the amplitudes (see Eq. A6 in Appendix). However, the relationships between the amplitudes remain the same if the depolarization ratios are kept equal. Following Williams and Dunker (3), we assume that the Raman polarizability tensor is nearly constant for the different structure types. Hence, the choice of arbitrary (but equal) depolarization ratios ρ^R for the bands in the amide I region does not influence the estimated contents of the secondary structure elements. To obtain more information on the actual values of the depolarization ratios of the Raman bands, the phase-mismatching (PMM) technique (29, 30) or nondegenerate PCARS (using three independent waves with different polarizations) may be proposed.

We can now compare our data with existing x-ray, Raman, CD, and Fourier transform infrared (FTIR) data (see Table 2). Although many authors used conformational subelements (e.g., ordered and unordered α-helices, parallel and antiparallel β-strands) in their fit procedures, all of them present data on the total content of the α-helical, β-sheet, and random coil conformations. Data obtained from PCARS spectra are in reasonable agreement with those obtained from the alternative methods (see Fig. 9 for the comparison of the PCARS and x-ray data). An exception forms lysozyme where the difference in the α-helical content is rather large. It is
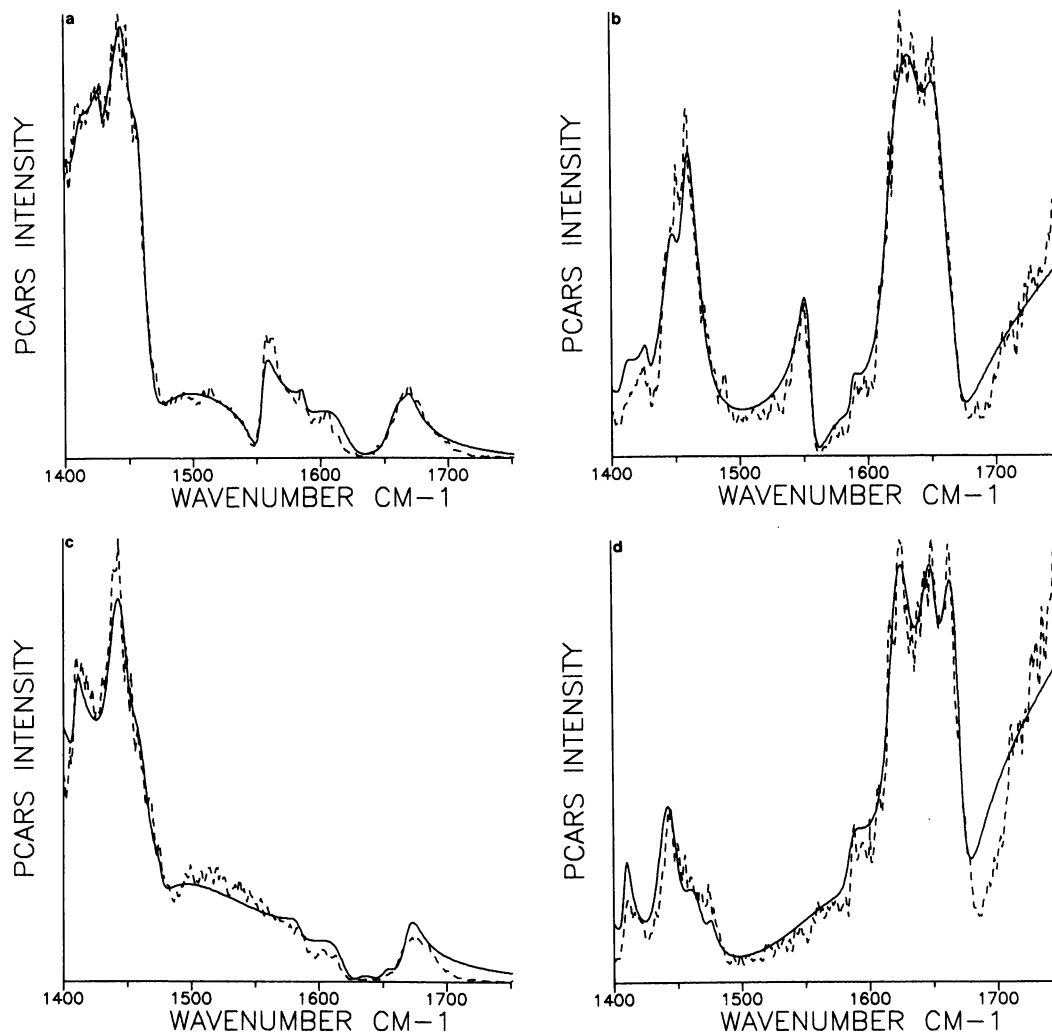
clear that application of PCARS for a precise estimation of the secondary conformation may be possible after increasing the signal to noise ratio. Also, PCARS spectra of other proteins or model polypeptides should be obtained.

The differences observed in Table 2 could be also due to different contributions from other subelements of the secondary conformation (e.g., ordered and unordered helices, parallel and antiparallel β-strands). These subelements may have different Raman spectra (see, for example, references 3–5, where the calculated spectra of the basic fitting set differ from each other significantly). It means that estimation of the content of α-helix or β-sheet is a formal procedure and is possible only after estimation of the contents of the subelements. From a spectroscopical point of view, it means that different elements contribute to different parts of the spectrum, and this may lead to the different results in the determination of secondary conformation by direct spectroscopic mea-

surements as used in our case. However, the fact that for all proteins studied the spectra in the amide I region are "split" by PCARS into three bands with almost the same frequencies and bandwidths may be interpreted as proof of the existence of three major groups of peptide bond conformations. It is well known that identification of the secondary conformational elements using x-ray data (to which almost all authors using Raman, CD, or Fourier transform infrared methods refer) is based on "grouping" of the amino-acid residues according to some criteria. Levitt and Greer (26), for example, used three methods (torsion angle, H-bond, and $C^\alpha - C^\alpha$ distance) for identification of the secondary conformation. In this respect, we may suppose that PCARS provides direct information on conformations in the protein molecule, although it is not quite clear now what spatial structures correspond to each of them. We think that this identification will be possible after obtaining additional data from PCARS of proteins with known conformations.

Ω	Γ	A a.u.	ρ^R	Assignment (27, 28)
cm^{-1}	cm^{-1}			
Albumine				
1409	4.6	13.5	0	His ?
1430	10.5	17.1	0	Trp
1450	7.4	45.4	0.75	CH$_2$-bending
1461	7.9	30.3	0.75	CH$_3$ asym def
1469	4.1	11.9	0.75	CH def, CH$_2$sym str
1587	3.7	8.7	0.75	Trp, Phe
1607	2.7	12.2	0.75	Phe
1612	12.0	10.1	0.75	Tyr, Phe, Trp
1638	12.6	30.1	0	α
1652	10.6	28.0	0	amide-I r.c.
1668	6.1	0.5	0	β
α-Chymotrypsin				
1426	2.0	4.1	0	Trp
1449	4.3	26.3	0.75	CH$_2$-bending
1460	8.0	29.1	0.75	CH asym def
1469	4.5	15.2	0.75	CH^3 def, CH$_2$sym str
1554	5.4	18.3	0	Trp
1587	3.7	6.5	0.75	Trp, Phe
1607	2.9	5.3	0.75	Phe
1614	15.3	13.1	0.75	Tyr, Phe, Trp
1639	10.8	8.2	0	α
1661	12.0	15.3	0	amide-I r.c.
1673	7.1	25.0	0	β
Lysozyme				
1409	5.1	5.7	0	His ?
1428	3.3	4.2	0.75	Trp
1448	8.0	19.4	0.75	CH$_2$-bending
1460	8.0	34.5	0.75	CH$_3$ asym def
1468	4.1	2.6	0.75	CH def, CH$_2$sym str
1553	5.4	31.2	0	Trp
1587	3.0	4.4	0.75	Trp, Phe
1615	14.7	16.3	0.75	Tyr, Phe, Trp
1637	12.9	13.7	0	α
1657	12.0	34.9	0	amide-I r.c.
1668	6.0	7.7	0	β
Ribonuclease A				
1409	3.5	15.1	0	His ?
1437	11.0	25.0	0	
1447	8.7	19.2	0.75	CH$_2$-bending
1463	11.0	23.0	0.75	CH$_3$ asym def
1475	4.4	6.2	0.75	CH def, CH$_2$sym str
1584	6.5	5.5	0.75	Phe
1617	11.7	16.0	0.75	Tyr, Phe
1630	10.1	12.6	0	α
1651	6.5	13.0	0	amide-I r.c.
1668	8.8	35.4	0	β

In the fitting procedure a depolarization ratio of 0 or 0.75 was assumed for the polarized or depolarized bands, respectively.

		Percent of total residues		
	Reference	α-Helix	β-Sheet	Random coil
Albumine				
PCARS	This work	52	1	47
Raman	(2)	60	0	40
CD	(25, 31)	54–62	0–3	41–51
α-Chymotrypsin				
PCARS	This work	17	51	32
X-ray	(26)	10	49	
Raman	(2)	4	34	62
CD	(32)	5	53	
Lysozyme				
PCARS	This work	24	14	62
X-ray	(26)	46	19	
Raman	(2)	32	9	59
Raman	(4)	47	19	
Raman	(5)	44	15	41
CD	(32)	32	29	
Ribonuclease A				
PCARS	This work	21	58	21
X-ray	(26)	22	46	
Raman	(2)	14	35	51
Raman	(4)	24	46	
CD	(32)	21	39	

promising in this respect and that it is worthwhile to continue such studies. The proposed methods for improving the signal to noise ratio (nondegenerate and phase mismatching PCARS) will be subject of our future work for the investigation of protein conformations in solution.
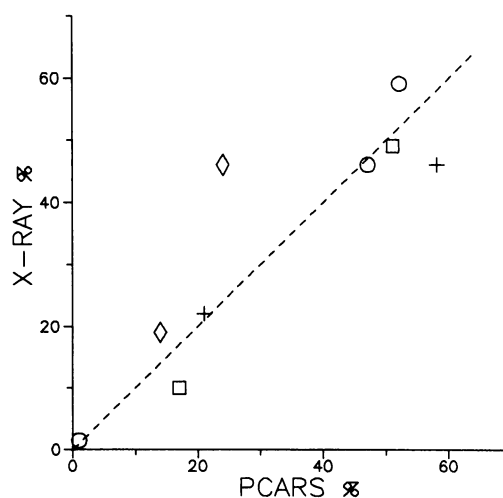

FIGURE 9 Correlation between x-ray (26) and PCARS (this work) data of α-helical, β-sheet, and random coil content in percents. The dashed line corresponds to 100% correlation. For albumin, averaged CD and Raman values are taken. O, albumin; □, α chymotrypsin; +, ribonuclease A; ◇, lysozyme.

It was stated in the introduction that one of our aims was to clarify if PCARS really gives direct spectroscopic information compared with existing spectroscopic techniques. We think that the results obtained are quite

APPENDIX

PCARS theory

The component i of the PCARS polarization vector is given by

$$P_i^{(3)} = \chi_{ijkl}^{(3)} e_j e_k e_l^* E_j E_k E_l^* \tag{A1}$$

where i, j, k, l = x, y or 1, 2. The dot * indicates that the photon is emitted.

For an isotropic medium, only three components, $\chi_{ijkl}^{(3)}$, are independent, the relation between them is expressed by

$$\chi_{1111}^{(3)} = \chi_{1122}^{(3)} + \chi_{1212}^{(3)} + \chi_{1221}^{(3)}. \tag{A2}$$

In degenerate PCARS, we have only two independent input polarization vectors $e_1 = e_p$ and $e_2 = e_s$; therefore, $\chi_{1122}^{(3)}$ and $\chi_{1212}^{(3)}$ are indistinguishable.

The projection of the CARS polarization vector on the analyzer unit vector is

$$e_A^* \cdot P^{(3)} = e_A^* \cdot ((\chi_{1122}^{(3)} + \chi_{1212}^{(3)}) e_1 (e_1 \cdot e_2^*)$$
$$+ \chi_{1221}^{(3)} e_2^* (e_1 \cdot e_1)) E_1^2 E_2^* \tag{A3}$$

Defining the depolarization ratio by

$$\rho = \frac{\chi_{1221}^{(3)}}{\chi_{1111}^{(3)}}, \tag{A4}$$

Eq. A3 can be rewritten using Eqs. A2 and A4

$$e_A^* \cdot P^{(3)} = \chi_{1111}^{(3)} ((1 - \rho)(e_A^* \cdot e_1)(e_1 \cdot e_2^*)$$
$$+ \rho(e_A^* \cdot e_2^*)) E_1^2 E_2^*. \tag{A5}$$

It follows for the total contribution of nonresonant and resonant susceptibilities to the CARS intensity I_A

$$I_A \sim |(e_A^* \cdot (\chi^{(3)N} + \chi^{(3)R}) E_1^2 E_2^*)|^2$$
$$= \left| f^N \chi^N + \sum_r f_r^R \frac{A_r}{-i - \Delta_r} \right|^2 I_1^2 I_2, \tag{A6}$$

where

$$\chi^N = \chi_{1111}^{(3)NR} \tag{A7}$$

$$\frac{A_r}{-i - \Delta_r} = \chi_{1111}^{(3)R,r} \tag{A8}$$

$$f^N = ((1 - \rho^N)(e_A^* \cdot e_1)(e_1 \cdot e_2^*) + \rho^N(e_A^* \cdot e_2^*)) \tag{A9}$$

$$f_r^R = ((1 - \rho_r^R)(e_A^* \cdot e_1)(e_1 \cdot e_2^*) + \rho_r^R(e_A^* \cdot e_2^*)) \tag{A10}$$

$$\rho^N = \frac{\chi_{1221}^{(3)NR}}{\chi_{1111}^{(3)NR}} \text{ nonresonant depolarization ratio} \tag{A11}$$

$$\rho_r^R = \frac{\chi_{1221}^{(3)R,r}}{\chi_{1111}^{(3)R,r}} \text{ vibration resonant depolarization ratio.} \tag{A12}$$

Assuming linear polarization vectors and defining the axes system as depicted in Fig. 4, the polarization factors f^N and f_r^R can be calculated in dependence on the angles α and ψ (or $\beta = \pi - (\alpha + \psi)$).

With α the angle between e_1 and e_2 and ψ the angle between e_1 and e_A,

$$f^N = ((1 - \rho^N) \cos \alpha \cos (\alpha + \psi) + \rho^N \cos \psi) \tag{A13}$$

$$f_r^R = ((1 - \rho_r^R) \cos \alpha \cos (\alpha + \psi) + \rho_r^R \cos \psi). \tag{A14}$$

Defining the angle between the polarization e_1 and $P^{NR,R}$ by $\theta^{NR,R}$, we can write

$$\tan \theta^{NR,R} = \left(\frac{P_y^{NR,R}}{P_x^{NR,R}} \right). \tag{A15}$$

It follows from Eqs. A3 to A5 that

$$\theta^{NR,R} = \arctan (\rho^{NR,R} \tan \alpha). \tag{A16}$$

Full suppression of the nonresonant polarization is achieved at angles ψ_0 or $\beta_0 = \pi - (\alpha + \psi_0)$, where $f^N = 0$ holds.

$$\psi_0 = \arctan \left[\frac{1}{\rho^N \tan \alpha} \right] \tag{A17}$$

$$\beta_0 = \arctan \left[\frac{\cos 2\alpha + \dfrac{1 + \rho^N}{1 - \rho^N}}{\sin 2\alpha} \right]. \tag{A18}$$

Assuming Kleinmann symmetry, $\psi_{1111}^{(3)}/3 = \chi_{1122}^{(3)} = \chi_{1212}^{(3)} = \chi_{1221}^{(3)}$, thus $\rho^N = \frac{1}{3}$ and Eq. 5 is valid.

REFERENCES

1. Yu, T. J., J. L. Lippert, and W. L. Peticolas. 1973. Laser Raman studies of conformational variations of poly-L-lysine. *Biopolymers.* 12:2161–2176.

2. Lippert, J. L., D. Tyminski, and P. J. Desmeules. 1976. Determination of the secondary structure of proteins by laser Raman spectroscopy. *J. Am. Chem. Soc.* 98:7075–7080.

3. Williams, R. W., and A. K. Dunker. 1981. Determination of the secondary structure of proteins from the amide I band of the laser Raman spectrum. *J. Mol. Biol.* 152:783–813.

4. Williams, R. W. 1983. Estimation of protein secondary structure from the laser Raman amide I spectrum. *J. Mol. Biol.* 166:581–603.

5. Berjot, M., J. Marx, and A. J. P. Alix. 1987. Determination of the secondary structure of proteins from the Raman amide I band: the reference intensity profiles method. *J. Raman Spectrosc.* 18:289–300.

6. Copeland, R. A., and T. G. Spiro. 1986. Ultraviolet Raman hypochromism of the tropomyosin amide modes: a new method for estimating α-helical content in proteins. *J. Am. Chem. Soc.* 108:1281–1285.

7. Marx, J., J. Jacquot, M. Berjot, E. Puchelle, and A. J. P. Alix. 1986. Characterization and conformational analysis by Raman spectroscopy of human airway lysozyme. *Biochim. Biophys. Acta.* 870:488–494.

8. Otto, C., F. F. M. de Mul, B. J. M. Harmsen, and J. Greve. 1987. A Raman scattering study of the helix-destabilizing gene-5 protein

with adenine containing nucleotides. *Nucleic Acids Res.* 15:7605–7625.

9. Pezolet, M., M. Pigeon, D. Menard, and J. P. Caille. 1988. Raman spectroscopy of cytoplasmic muscle fiber proteins. *Biophys. J.* 53:319–325.

10. Byler, D. M., and H. Susi. 1986. Examination of the secondary structure of proteins by deconvolved FTIR spectra. *Biopolymers.* 25:469–487.

11. Krimm, S. 1962. Infrared spectra and chain conformation of proteins. *J. Mol. Biol.* 4:528–540.

12. Chikishev, A. Y. 1987. Application of spontaneous Raman and CARS to the study of enzyme action. *In* Laser Scattering Spectroscopy of Biological Objects. J. Stepanek, P. Anzenbacher, and B. Sedlacek, editors. Elsevier, New York. 309–316.

13. Chikishev, A. Y., V. F. Kamalov, N. I. Koroteev, V. V. Kvach, A. P. Shkurinov, and B. N. Toleutaev. 1988. Time resolved spontaneous and coherent Raman scattering of Ni-octaethyl-porphyrin in excited electronic states. *Chem. Phys. Lett.* 144:90–95.

14. Duncan, M. D., J. Reintjes, and T. S. Manuccia. 1982. Scanning coherent anti-Stokes Raman microscope. *Optics Lett.* 7:350–352.

15. Dutta, P. K., R. Dallinger, and T. G. Spiro. 1980. Resonance CARS line shapes via Frank-Condon scattering: cytochrome *c* and *β*-carotene. *J. Chem. Phys.* 73:3580–3585.

16. Nestor, J., T. G. Spiro, and G. Klauminzer. 1976. Coherent anti-Stokes Raman scattering (CARS) spectra with resonance enhancement of cytochrome c and vitamine B_{12} of dilute aqueous solution. *Proc. Natl. Acad. Sci. USA.* 73:3329–3332.

17. Payne, S. A., and R. M. Hochstrasser. 1986. Picosecond transient coherent anti-Stokes Raman spectroscopy of rhodamine 560 in ethanol. *Optics Lett.* 11:285–287.

18. Scholten, T. A. H. M., G. W. Lucassen, F. F. M. de Mul, and J. Greve. 1989. Possibilities and limitations of off-resonance polarization sensitive CARS of short chain proteins. *Optics. Comm.* 72:328–334.

19. Trommsdorff, H. P., J. R. Andrews, and R. M. Hochstrasser. 1982. Excited state vibrational spectroscopy by multi-resonant four wave mixing. *Appl. Phys.* B28:147–148.

20. Akhmanov, S. A., and N. I. Koroteev. 1981. Methods of Nonlinear Optics in the Light Scattering Spectroscopy. Nauka, Moscow.

21. Ivanov, A. A., N. I. Koroteev, and A. I. Fishman. 1991. Coherent holographic spectroscopy of molecules. *In* Laser Applications in Life Sciences. SPIE—The International Society for Optical Engineering. S. A. Akhmanov and M. Yu. Poroshina, editors. 174–184.

22. Koroteev, N. I. 1987. Interference phenomena in coherent spectroscopy of scattering and absorption of light: holographic multi-dimensional spectroscopy. *Sov. Phys. Usp.* 30:628–642.

23. Blout, E. R., C. DeLoae, and A. Asadourian. 1961. The deuterium exchange of water-soluble polypeptides and proteins as measured by infrared spectroscopy. *J. Am. Chem. Soc.* 83:1895.

24. Scholten, T. A. H. M., G. W. Lucassen, F. F. M. de Mul, and J. Greve. 1988. Compensating pulse-to-pulse fluctuations and increasing spectral reproducibility of phase-matched CARS measurements. *Appl. Opt.* 27:3225–3231.

25. Greenfield, N., and G. D. Fasman. 1969. Computed circular dichroism spectra for the evaluation of protein conformation. *Biochemistry.* 8:4108.

26. Levitt, M., and J. Greer. 1977. Automatic identification of secondary structure in globular proteins. *J. Mol. Biol.* 114:181–293.

27. Lord, R. C., and N. T. Yu. 1970. Laser-excited Raman spectroscopy of biomolecules. *J. Mol. Biol.* 51:203–213.

28. Otto, C. 1987. Raman and surface enhanced Raman spectroscopy of Helix destabilizing proteins and nucleotides. Ph.D. thesis. University of Twente, Enschede, The Netherlands.

29. Lucassen, G. W., T. A. H. M. Scholten, W. P. de Boeij, F. F. M. de Mul, and J. Greve. 1991. Nonresonant background suppression in CARS spectra of dissolved molecules. *In* Laser Applications in Life Sciences. S. A. Akhmanov and M. Yu. Poroshina, editors. 185–194.

30. Scholten, T. A. H. M., G. W. Lucassen, F. F. M. de Mul, and J. Greve. 1989. Nonresonant background suppression in CARS spectra of dispersive media using phase mismatching. *Appl. Opt.* 28:1387–1400.

31. Barela, T. D., and D. W. Darnall. 1974. Practical aspects of calculating protein secondary structure from circular dichroism. *Biochemistry.* 13:1694.

32. Chang, C. T., C. S. Wu, and Y. T. Yen. 1978. Circular dichroic analysis of protein conformation: inclusion of the *β*-turns. *Anal. Biochem.* 91:13–31.